Soft Matter

PAPER

View Article Online
View Journal

Cite this: DOI: 10.1039/d0sm01220c

Revisiting the emergence of order in active matter†

Oleksandr Chepizhko, [a] David Saintillan [b] and Fernando Peruani *[c]

Received 3rd July 2020,
Accepted 9th February 2021

DOI: 10.1039/d0sm01220c

rsc.li/soft-matter-journal

The emergence of orientational order plays a central role in active matter theory and is deeply based in the study of active systems with a velocity alignment mechanism, whose most prominent example is the so-called Vicsek model. Such active systems have been used to describe bird flocks, bacterial swarms, and active colloidal systems, among many other examples. Under the assumption that the large-scale properties of these models remain unchanged as long as the polar symmetry of the interactions is not affected, implementations have been performed using, out of convenience, either additive or non-additive interactions; the latter are found for instance in the original formulation of the Vicsek model. Here, we perform a careful analysis of active systems with velocity alignment, comparing additive and non-additive interactions, and show that the macroscopic properties of these active systems are fundamentally different. Our results call into question our current understanding of the onset of order in active systems.

1 Introduction

The building blocks of what we typically call active matter[1,2] —*i.e.*, autonomous, self-propelled particles (SPPs)—can be either biological entities or man-made physical objects. Biological examples of SPPs are abundant and found across scales, from microscopic *in vitro* cytoskeletal extracts,[3–5] collections of swimming[6–9] and gliding[10,11] bacteria, motile cell cultures[12,13] to macroscopic bird flocks and animal herds.[14,15] The number of fabricated, physical SPPs remains comparatively smaller, but examples are rapidly growing and include at the sub-micron scale active colloidal particles[16–20] and active rollers,[21–23] and at larger scales (*e.g.*, centimeter scale) vibrated, self-propelled, granular rods[24,25] and disks[26] as well as robots.[27]

Several of these active systems, but not all of them,[28] display spectacular collective effects resulting from velocity–velocity alignment interactions. For physical active systems such as ref. 21–23 and 26, such velocity alignment interactions have been derived from first-principle arguments. In living active systems, the inherent biological complexity of the individuals, which may include biochemical signaling mechanisms among other highly nontrivial features, prevents a direct derivation of the interactions among the individuals. However, for small, unicelullar organisms, such as bacteria, physical interactions—*e.g.*, steric or hydrodynamic interactions—dominate over biological ones during processes such as collective motion. For these systems, it was argued that pairwise additive velocity alignment interactions are consistent with the empirical observations,[29–32] and experimental measurements have provided solid evidence in favor of such arguments.[10,33]

The situation is substantially more critical in larger organisms such as fish, birds, or sheep, where interactions are the result of complex cognitive processes and not the mere result of physical interactions. Certainly, there is no reason to believe that the functional form of the interactions in these systems is identical to that for bacteria or colloidal rollers. In biological systems, interactions are often not additive and microscopic details matter. More specifically, the biological response of an organism subject to a stimulus tends to saturate and does not grow unboundedly with stimulus strength. While the stimulus may be proportional to the number of neighbors, the response of the organism, which may rely on biochemical signaling or cognitive processes, typically is not. This is in sharp contrast to the pairwise additive interactions used in the description of *e.g.*, gravitational or electrostatic (classical) systems.

Flocking models with velocity alignment such as the Vicsek model[34] have been implemented with both additive and non-additive interactions[1,2,35–37] and applied to describe living as well as non-living active matter.[1,2] In the literature,

[a] *Institut für Theoretische Physik, Universität Innsbruck, Technikerstraße 21A, A-6020 Innsbruck, Austria*
[b] *Department of Mechanical and Aerospace Engineering, University of California San Diego, 9500 Gilman Drive, La Jolla, CA 92093-0411, USA*
[c] *Laboratoire de Physique Théorique et Modélisation, UMR 8089, CY Cergy Paris Université, 95302 Cergy-Pontoise, France. E-mail: fernando.peruani@cyu.fr*

† Electronic supplementary information (ESI) available: movie1.mov – Momentum non-conserved, $N = 90\,000$, $L = 300$, $\eta = 0.72$. Clear stable band emerges. movie2.mov – Momentum conserved, $N = 90\,000$, $L = 300$, $\eta = 0.01$. Evolution from initial uniformly distributed state to coarsened clusters. movie3.mov – Momentum conserved, $N = 90\,000$, $L = 300$, $\eta = 1.3$. Evolution from uniformly distributed initial state to a state with correlated clusters. movie4.mov – Momentum conserved, $N = 90\,000$, $L = 300$, $\eta = 1.8$. Evolution from uniformly distributed initial state to a state with correlated clusters. For all movies, $R_0 = 1$ and $\rho = 1$. See DOI: 10.1039/d0sm01220c

the choice between additive and non-additive interactions in flocking models seems to be made mainly based on convenience, with additive interactions being preferable when it comes to analytical treatments and non-additive interactions allowing for faster and more reliable numerical schemes. The underlying assumption is that active models with the same interaction symmetry—specifically, polar (or ferromagnetic) symmetry—exhibit qualitatively identical large-scale properties. Yet, active systems are intrinsically non-equilibrium systems and there is no fundamental reason why additive and non-additive interactions should produce the same dynamics, even if they share the same symmetry. Here, we perform a detailed comparison of active systems with velocity-alignment with additive and non-additive interactions. Using a combination of agent-based simulations and mean-field modeling, we show that the large-scale properties of the ordered phases strongly depend on whether interactions are either additive or non-additive, as well as on boundary conditions. The obtained collection of results calls into question our current theoretical understanding of the emergence of order in active systems.

2 Flocking models

We consider ensembles of N self-propelled particles that move at constant speed in a two-dimensional space, using either periodic or reflecting boundary conditions. Reflecting conditions are implemented as specular reflections as particles hit the circular wall, *i.e.*, the sign of the velocity component normal to the wall is changed, while the component parallel to it remains untouched. In the overdamped limit, we express the temporal evolution of the position of the i-th particle by:

$$\dot{\mathbf{x}}_i = \mathbf{V}(\theta_i), \tag{1}$$

where $\mathbf{V}(\cdot) \equiv \cos(\cdot)\hat{\mathbf{x}} + \sin(\cdot)\hat{\mathbf{y}}$, and the angle θ_i defines the direction of motion of the particle. As in most flocking models, we assume a velocity alignment mechanism, *i.e.*, an interaction that favors alignment of the velocities of neighboring particles. The dynamics of the moving direction θ_i, which contains the alignment rule, obeys:

$$\dot{\theta}_i = \sum_{j=1}^{N} J_{i,j} + \sqrt{2D}\xi_i(t), \tag{2}$$

where $\xi_i(t)$ refers to a white noise term such that $\langle \xi_i(t) \rangle = 0$, $\langle \xi_i(t)\xi_j(t') \rangle = \delta_{i,j}\delta(t-t')$, and noise amplitude $\eta \equiv \sqrt{2D}$ (leading, in absence of interactions, to an angular diffusion D). The interaction term $J_{i,j}$ is defined differently for additive and non-additive interactions. Together with eqn (1), this leads to the two most commonly used implementations of vectorial active matter[21,22,35–39]—often misleadingly referred to as (continuum-time) Vicsek-like models—namely:

$$\dot{\theta}_i = \begin{cases} \sum\limits_{\Omega_i} \sin(\theta_j - \theta_i) + \sqrt{2D}\xi_i(t) & \text{for additive interactions,} \\ \dfrac{1}{n_i}\sum\limits_{\Omega_i} \sin(\theta_j - \theta_i) + \sqrt{2D}\xi_i(t) & \text{for non-additive interactions,} \end{cases}$$

where Ω_i is the set of neighbors of particle i and n_i the number of particles contained in Ω_i. It is useful to express $J_{i,j}$ as follows:

$$J_{i,j} = K(\mathbf{x}_i,\mathbf{x}_j)\sin(\theta_j - \theta_i). \tag{3}$$

The kernel K determines the neighborhood of particle i and $\sin(\theta_j - \theta_i)$ dictates the symmetry of the interactions—here polar (or ferromagnetic). In the following, we discuss the two standard functional forms for $K(\mathbf{x}_i,\mathbf{x}_j)$ that have been repeatedly used in the active matter literature: (a) $K(\mathbf{x}_i,\mathbf{x}_j)$ was defined as $K(\mathbf{x}_i,\mathbf{x}_i) = H(R_0 - |\mathbf{x}_i - \mathbf{x}_j|)$ in *e.g.* ref. 21, 22, 35, 36 and 38, with $H(\cdot)$ a Heaviside step function ($H(h) = 1$ for $h > 0$ and $H(h) = 0$ otherwise) and R_0 a constant that determines the interaction radius. Since $K(\mathbf{x}_i,\mathbf{x}_j)$ depends on the distance between $\mathbf{x}_i$ and $\mathbf{x}_j$, $K(\mathbf{x}_i,\mathbf{x}_j) = K(\mathbf{x}_j,\mathbf{x}_i)$ and interactions are pairwise additive. (b) $K(\mathbf{x}_i,\mathbf{x}_j)$ was defined as $K(\mathbf{x}_j,\mathbf{x}_i) = H(R_0 - |\mathbf{x}_i - \mathbf{x}_j|)/n(\mathbf{x}_i)$, where $n(\mathbf{x}_i) = \sum_{j=1}^{N} H(R_0 - |\mathbf{x}_j - \mathbf{x}_i|)$ refers to the number of neighbors of particle i, in ref. 37 and 39. Using this definition, $\sum_j J_{i,j} = \frac{1}{n(\mathbf{x}_i)}\sum_j H(R_0 - |\mathbf{x}_j - \mathbf{x}_i|)\sin(\theta_j - \theta_i)$. The non-additivity is evident in this notation, where the interaction rule appears explicitly as a local average. Thus, the temporal evolution of θ_i is independent of the number of neighbors. As discussed above, this is a desirable property if the self-propelled entities display a bounded turning speed as a result, for instance, of limited reflex responses and/or muscular forces, among other possibilities. Note that since the interaction strength with neighboring particle j depends on the total number of neighbors $n(\mathbf{x}_i)$, which in turn involves a sum over all the neighboring particles, it is not possible to write the interaction rule as a simple sum of pair interactions that depend exclusively on the state of the involved pairs. The consequences of this non-additivity are far-reaching as we explain below. As particles i and j generally have different numbers of neighbors, *i.e.* $n(\mathbf{x}_i) \neq n(\mathbf{x}_j)$, then $K(\mathbf{x}_i,\mathbf{x}_j) \neq K(\mathbf{x}_j,\mathbf{x}_i)$.

When $K(\mathbf{x}_i,\mathbf{x}_j) = K(\mathbf{x}_j,\mathbf{x}_i)$, *i.e.* for the functional form (a), since $\sin(\theta_j - \theta_i) = -\sin(\theta_j - \theta_i)$, it is evident that $J_{i,j} = -J_{j,i}$. This implies that $\left\langle \sum_{i=1}^{N} \dot{\theta}_i \right\rangle = \left\langle \sum_{i,j} J_{i,j} \right\rangle + \eta \sum_i \langle \xi_i(t) \rangle = 0$, and, in consequence, these additive interactions, as defined, conserve angular momentum in the sense indicated above. In the following, we refer to these interactions as MC (momentum-conserving) interactions. On the other hand, when $K(\mathbf{x}_i,\mathbf{x}_j) \neq K(\mathbf{x}_j,\mathbf{x}_i)$ (functional form (b)), then $J_{i,j} \neq -J_{j,i}$, and specifically $J_{i,j} + J_{j,i} = H(R_0 - |\mathbf{x}_j - \mathbf{x}_i|)\sin(\theta_j - \theta_i)[n(\mathbf{x}_i)^{-1} - n(\mathbf{x}_j)^{-1}]$. It is thus evident that the action-reaction principle is not fulfilled, implying that many commonly used flocking models belong to the class of active systems with non-reciprocal interactions, even though the non-reciprocity is not explicitly evident from the model

definition.[28,40] Furthermore, the found asymmetry implies that $\left\langle \sum_{i=1}^{N} \dot{\theta}_i \right\rangle \neq 0$. Therefore, non-additive velocity alignment does not conserve angular momentum (in the sense indicated above), and in the following, we refer to these interactions as NMC.

It is worth noting that the celebrated Vicsek model[34] was formulated in an algorithmic fashion and in such a way that particles at each time step Δt, and independently of the number of neighbors, adopt the average local direction of motion. As such, it is clear that the Vicsek model falls in the category of NMC interactions. This means that a correct continuous-time version of the Vicsek model should possess NMC interactions as in ref. 37 and not MC interactions as in flocking models studied in ref. 35, 36 and 38. We insist that though it has been repeatedly assumed that flocking models with NMC and MC interactions display the same behavior,[21,22,35,36,38] the large-scale properties of active systems with NMC and MC interaction are, as explained below, fundamentally different.

3 Mean-field theory

Differences between MC and NMC interactions are straightforward to analyze and identify theoretically at the mean-field (MF) level. Since the equations of motion are given by Langevin equations,[41] the MF is derived from the non-linear Fokker–Planck equation associated to eqn (2), which reads:

$$\partial_t p = -\partial_\theta \left[\Gamma(\rho) \int_0^{2\pi} \mathrm{d}\theta' \sin(\theta' - \theta) p(\theta') p(\theta) \right] + D \partial_{\theta\theta} p, \qquad (4)$$

where $p(\theta) = p(\theta,t)$ and $D = \eta^2/2$. Assuming a homogeneous distribution of particles such that $\rho(\mathbf{x}) = \rho$ with $\rho = N/L^2$, the function $\Gamma(\rho)$ is directly related to $K(\mathbf{x},\mathbf{x}')$ by $\Gamma(\rho) = \int_\Omega \mathrm{d}\mathbf{x}' \rho(\mathbf{x}') K(\mathbf{0},\mathbf{x}') = \pi R_0^2 \rho$ for MC. For NMC, given that by definition $\Gamma(\rho) = \left[\int_\Omega \mathrm{d}\mathbf{x}' \rho(\mathbf{x}') K(\mathbf{0},\mathbf{x}')\right] / n(\mathbf{0})$ with $n(\mathbf{0}) = \int_\Omega \mathrm{d}\mathbf{x}' \rho(\mathbf{x}') K(\mathbf{0},\mathbf{x}') = \pi R_0^2 \rho$, we obtain $\Gamma(\rho) = 1$. The steady-state solution of eqn (4), assuming a constant density ρ is:

$$p_{\mathrm{st}}(\theta) = \mathcal{N} \exp\left[\frac{\Gamma(\rho) \langle v \rangle \cos(\theta - \psi)}{D} \right], \qquad (5)$$

where $\mathcal{N}$ is a normalization constant, ψ denotes the direction in which the rotational symmetry was broken, and $\langle v \rangle$ is the orientational order parameter defined as:

$$\langle v \rangle = \left| \int_0^{2\pi} \mathrm{d}\theta p_{\mathrm{st}}(\theta) \exp(i\theta) \right|. \qquad (6)$$

Note that the expression given by eqn (5) depends on $\langle v \rangle$, which according to eqn (6) is computed using $p_{\mathrm{st}}(\theta)$. In short, this leads to a self-consistency relation between $\langle v \rangle$ and $p_{\mathrm{st}}(\theta)$, which can be expressed as $\langle v \rangle = I_1\left[\frac{\Gamma(\rho)\langle v \rangle}{D}\right] \Big/ I_0\left[\frac{\Gamma(\rho)\langle v \rangle}{D}\right]$, where $I_n[.]$ is the n-th order modified Bessel function of the first kind. From this expression we learn that at the mean-field level, the system exhibits a phase transition. This is particularly easy to observe by performing a Taylor expansion on the self-consistency relation and expressing it as $\langle v \rangle \approx \left(1 - \frac{\Gamma(\rho)^2}{(2D)^2} \frac{\langle v \rangle^2}{2}\right) \frac{\Gamma(\rho)}{2D} \langle v \rangle$. Above a given critical point, the only solution is $\langle v \rangle = 0$, while below it a second solution exists: $\langle v \rangle = 2^{3/2} D \sqrt{\frac{\Gamma(\rho) - 2D}{\Gamma(\rho)^3}}$. Inserting the definition of $\Gamma(\rho)$ given above, we find that the critical value D_{c} takes the form:

$$D_{\mathrm{c}}(\rho) = \begin{cases} \pi R_0^2 \rho / 2 & \text{for MC,} \\ 1/2 & \text{for NMC.} \end{cases} \qquad (7)$$

Eqn (7) predicts that the phase diagram in the D–ρ space differs between MC and NMC. In particular, for a fixed value of D, there is a critical density $\rho_{\mathrm{c}} = 2D/(\pi R_0^2)$ above which order emerges for MC, while such density dependency is not present for NMC and order requires, according to the MF, $D < 1/2$. Fig. 1, panels (a) and (e), compares results from agent-based simulations (symbols) with the MF predictions (black curves). For large ρ values, there exists a reasonable agreement between simulations and eqn (7); the MF is supposed to be exact in the limit $\rho \to \infty$. On the other hand, for small ρ values we observe a significant deviation between MF predictions and simulations for NMC. The qualitative behavior of $D_{\mathrm{c}}(\rho)$ obtained in simulations for dilute systems for MC and NMC is remarkably comparable: the dependency of the critical point D_{c} with ρ is evident for both type of interactions, with $D_{\mathrm{c}}(\rho)$ being an increasing function of ρ.

4 Fluctuations, finite size analysis and orientational order

The differences found at the MF level may have a farther-reaching impact than simply affecting the (non-universal) shape of $D_{\mathrm{c}}(\rho)$. The MF is expected to provide a reasonable description of the local dynamics of the system, but not necessarily, as very often occurs, of its macroscopic dynamics. According to the MF, for MC interactions, local density fluctuations above ρ_{c} induce local order. It is then expected that there exists a positive correlation between local order $\langle v \rangle_\ell$ and local density ρ_ℓ in the ordered and as well as disordered phase (*i.e.*, for all D values), which is confirmed in simulations as shown in the rightmost panel in the upper row in Fig. 2. Local order $\langle v \rangle_\ell$ is obtained by subdividing the system into cells of area $\ell \times \ell$ and computing for each cell k: $\langle v(k) \rangle_\ell = \left| \left(\left(\sum_{j \in \Omega(k,\ell)} \mathbf{V}(\theta_j) \right) \Big/ n(k,\ell) \right) \right|$, where $\Omega(k,\ell)$ is a set that contains all particles in the k-th cell and $n(k,\ell)$ is the number of particles in the cell, while the local density is given by $\rho_\ell(k) = n(k,\ell)/\ell^2$: each dot in Fig. 2 corresponds to a pair $[\langle v(k) \rangle_\ell, \rho_\ell(k)]$. Note that local order propagates ballistically, either recruiting other particles in its way or decaying away. On the other hand, for NMC, local density fluctuations cannot, at the MF level, lead to local order. However, by direct numerical integration of the system with NMC interactions, we observe the emergence of a (local) order-density coupling, *i.e.*, a positive correlation between of $\langle v \rangle_\ell$ with ρ_ℓ, in the ordered phase;

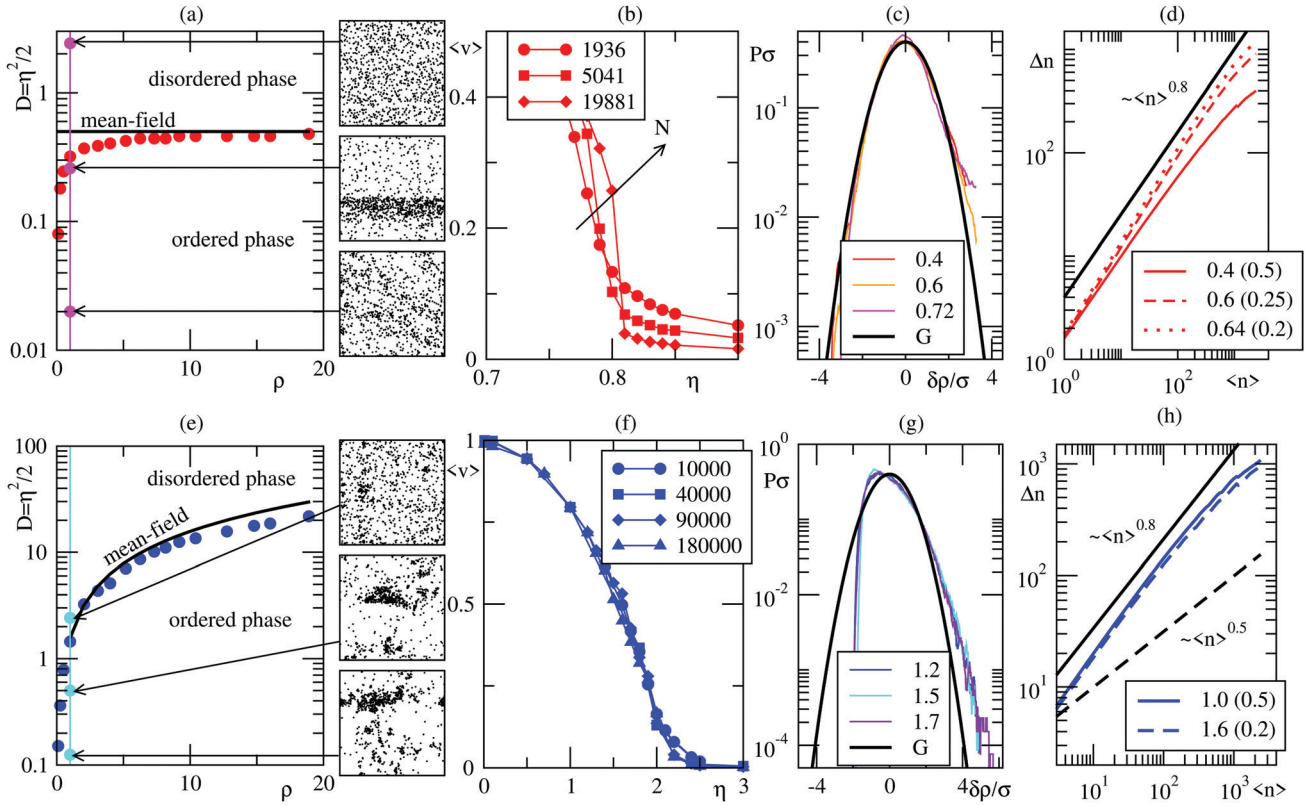

Fig. 1 Differences between NMC (top) and MC (bottom) interactions using periodic boundary conditions. From left to right: (a and e) phase diagram in the $D-\rho$ space with snapshots of corresponding phases; (b and f) order parameter $\langle v\rangle$ *vs.* noise strength η for various system sizes N; (c and g) probability of local density fluctuations $\delta\rho$ (for $\ell \sim R_0$) and (d and h) number fluctuations Δn *vs.* $\langle n\rangle$ for various η values (the relative noise strength $\xi = (\eta_c - \eta)/\eta_c$ is provided in parentheses). In all panels except (a) and (e), we use $R_0 = 1$ and $\rho = 1$.

see middle panel in the bottom row in Fig. 2. Such an order-density coupling for NMC must necessarily arise from a different mechanism than the one observed for MC that is already present at MF level: arguably, it results from the density dependency of macroscopic order fluctuations.[42] In summary, the observed differences at MF level suggest that fluctuations operate differently for MC and NMC interactions, and thus the macroscopic behavior of the system is likely to be different. To assess the role of fluctuations on the large-scale properties of MC and NMC systems, we perform a detailed finite-size study of the orientational order with periodic as well as reflecting boundary conditions.

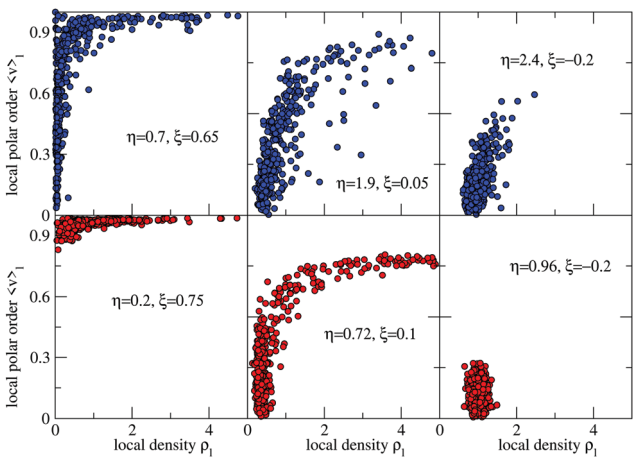

Fig. 2 Local order parameter $\langle v\rangle_\ell$ *vs.* local density ρ_ℓ for MC (upper row) and NMC (bottom row) interactions. The right most panel, for both rows, corresponds to the globally disordered phase, while the first (from left to right) two panels are computed in the globally ordered phase. Parameters are as in Fig. 1, global density $\rho = 1$ and $\ell = 14$.

Periodic boundary conditions

The global order parameter in simulations with periodic boundary conditions is defined as:

$$\langle v\rangle = \left|\frac{1}{N}\sum_{k=1}^{N}\mathbf{V}(\theta_k)\right| = \left|\frac{1}{N}\sum_{k=1}^{N}\exp(i\theta_k)\right|. \qquad (8)$$

The behavior of $\langle v\rangle$ as a function of $\eta = \sqrt{2D}$ indicates that the transition becomes sharper with system size for NMC, suggesting a first-order transition; see Fig. 1(b). This sharpening is not observed for MC interactions, see Fig. 1(b), but its absence *per se* does not rule out a first-order transition. By fixing the noise intensity η and varying the system size N while keeping the density ρ constant, we observe that for $D < D_c$, $\lim_{N\to\infty}\langle v\rangle \to \langle v\rangle_\infty$, where $\langle v\rangle_\infty > 0$ is a function of D that represents the value of the order parameter in an infinite system; see Fig. 3 where $\rho = 1$ and $D_c \sim 2$ for MC, while $D_c \simeq 0.32$ for NMC. These results indicate

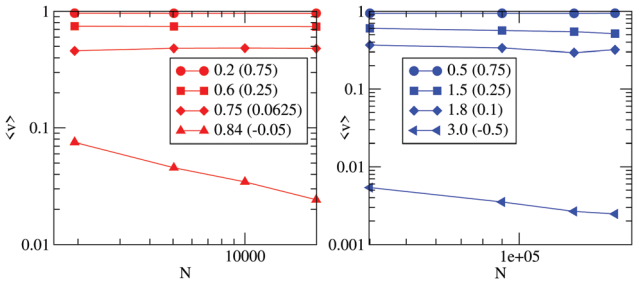

Fig. 3 Finite-size scaling of $\langle v \rangle$ with system size N for various noise amplitudes η for periodic boundary conditions. The legends refer to η; the relative noise intensity is indicated in parentheses. Left panel: NMC, and right panel: MC interactions. Parameters are as in Fig. 1.

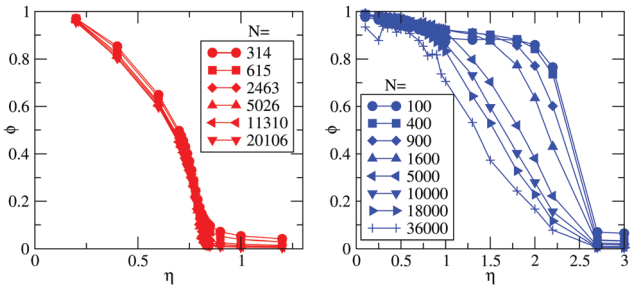

Fig. 5 Order parameter ϕ *vs.* noise amplitude η for various systems sizes using reflecting boundary conditions. Left: NMC interactions, right: MC interactions. Parameters are as in Fig. 1.

that MC and NMC with periodic boundary conditions exhibit a transition to order and that the emergent order is long-range (LRO) for NMC as well as MC.

Reflecting boundary conditions

In confined circular geometries with reflecting boundary conditions, we expect any emergent self-organized flow in the system to take the form of a vortex pattern. Thus, a high degree of order in a circular container should involve a collective rotation with a large number of particles rotating in the same direction; Fig. 4(a) and (c) for NMC and MC, respectively. In this case, we quantify orientational order using the parameter ϕ defined as

$$\phi = \left| \frac{1}{N} \sum_{k=1}^{N} \mathbf{V}(\alpha_k) \times \mathbf{V}(\theta_k) \right| = \left| \frac{1}{N} \sum_{k=1}^{N} \sin(\alpha_k - \theta_k) \right|, \qquad (9)$$

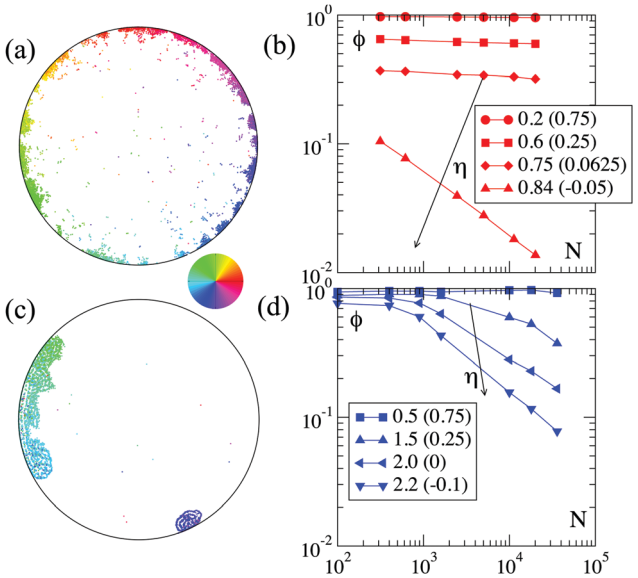

Fig. 4 Differences between NMC (top) and MC (bottom) interactions in confined systems with reflecting boundary conditions. (a) and (c) show snapshots of NMC and MC, respectively, where the particle orientation is color-coded. The finite-size scaling of the order parameter ϕ *vs.* N for different values of η is shown in (b) for NMC and in (d) for MC. The corresponding noise values are given in the legends; the relative noise strength ξ is given in parentheses. Parameters are as in Fig. 1.

where α_k is the polar angle associated with the position of particle k in polar coordinates: $\mathbf{x}_k = r_k \mathbf{V}(\alpha_k)$, with r_k the distance from the center of the container. The behavior of the order parameter ϕ as function of η, as well as the finite size behavior of ϕ with N, exhibit, in contrast to what we observed for periodic boundary conditions, strikingly differences between MC and NMC in confined geometries; Fig. 4 and 5. The curves ϕ *vs.* η using different system sizes indicate that the critical point ($\eta_c \sim 0.8$ for $\rho = 1$) remains the same if we use either periodic or reflecting boundary conditions for NMC interactions; Fig. 5. Furthermore, we find that in reflecting boundary condition, NMC interactions lead to an emergent order such that $\phi \propto N^{-\zeta(\eta)}$ with $\zeta(\eta) \leq 1/16$ for $\eta < \eta_c$ [Fig. 4(d)], suggesting quasi-long range order (QLRO), in sharp contrast to the LRO observed in periodic geometries. On the other hand, finite size effects for MC interactions using reflecting boundary conditions are even more dramatic. The behavior of $\phi(\eta)$ is highly sensitive to system size N as shown in Fig. 5. The emergent order decays algebraically with N as: $\phi \propto N^{-\zeta(\eta)}$ with $1/2 \geq \zeta(\eta) \gg 1/16$ for $\eta > 1$, which is a clear indication that the system is disordered; Fig. 4(d). It is only for values of $\eta < 1$ that the numerical data displays a slow decay consistent with QLRO. However, we speculate, from the behavior displayed by $\phi(\eta,N)$ for $\eta > 1$, that a crossover towards an exponent $\zeta(\eta) > 1/16$ will be observed at larger system sizes even for $\eta < 1$.

In summary, using periodic boundary conditions, both MC and NMC interactions lead to LRO; Fig. 3. With the reflecting boundary condition, finite size effects are fundamentally different and orientational order decays algebraically with system size. Furthermore, we observe qualitatively distinct behaviors with system size N for MC and NMC interactions. For NMC, the emergent order is QLRO, meaning $\zeta(\eta) \leq 1/16$, while for MC the order parameter ϕ decays much faster, which suggests that the system is disordered.

5 Bands and density fluctuations

There are other evident differences between MC and NMC interactions beyond those reported in relation to orientational order. For NMC interactions in periodic domains, self-propelled particles spontaneously organize into high-density structures called "bands" near the critical point. For an illustration of band dynamics with NMC interactions, see movie 1 (ESI†).

These bands are equivalent to the ones found in the discrete-time Vicsek model.[43] On the other hand, for MC interactions in periodic domains, bands are not observed, neither near the critical point nor well in the order phase. For MC interactions, particles self-organize into highly correlated moving clusters that by chance, at some point in time, may get placed in space roughly in line, providing the visual illusion of being observing a polar band. However, clusters quickly disconnect and deform and this visual illusion quickly dissolves. For an illustration of the dynamics of these highly correlated moving clusters with MC interactions, see movie 2, movie 3, and movie 4 (ESI†). Note that the emergence of bands in the Vicsek model has been explained by postulating in a spatially extended mean-field model a (local) order-density coupling.[44] Such an assumption certainly applies at the MF level to MC interactions, but not to NMC ones. However, counterintuitively bands are clearly observed of NMC, but not for MC interactions. This indicates that a (local) order-density coupling is not a sufficient—though likely to be necessary—condition for band formation. In the following, we show that the spatial organization and density fluctuations are fundamentally different in active systems involving MC and NMC interactions.

The first indication is provided by the probability $p(\delta\rho)$ of finding a local density fluctuation of amplitude $\delta\rho$. This is measured by subdividing the space into cells of area $\ell \times \ell$ and computing $\delta\rho = \rho_\ell - \langle\rho_\ell\rangle$ in each cell, where ρ_ℓ is the density in the cell and $\langle\rho_\ell\rangle$ its average over all cells. Fig. 1(c and g) shows that the functional form of $p(\delta\rho)$ below the critical point is qualitatively different for MC and NMC, with large fluctuations occurring more frequently in MC systems. On the other hand, and following a similar procedure, we find that the number density fluctuations $\Delta n = \sqrt{\langle(n(i,\ell) - \langle n\rangle)^2\rangle}$, with $n(i,\ell)$ the number of particles in cell i and $\langle n\rangle = \rho\ell^2$, are giant in both systems and with similar exponents; see Fig. 1(d and h).

The second indication of a qualitative difference in behavior is obtained by analyzing the projected density of the particles. The procedure is as follows. As illustrated in Fig. 6(a and b),

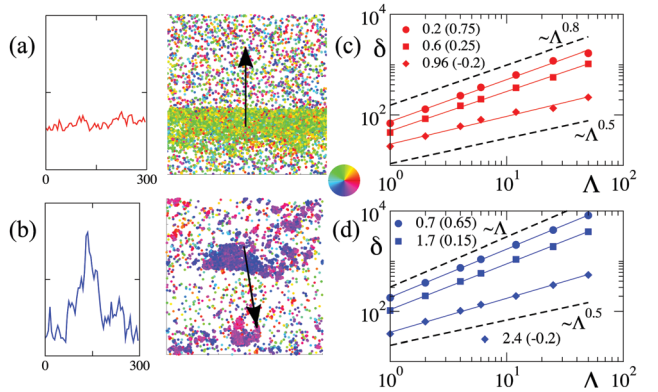

Fig. 6 (a) Projected density onto the direction orthogonal to the global moving direction and corresponding snapshot for NMC in periodic sytems; (b) same for CM. Particle orientations are color-coded. The arrow indicates the global direction of motion. (c) and (d) δ *vs.* Λ; see text for definitions. The data is given for different values of noise strength η (relative noise strength ξ in parentheses). Red lines in (c) correspond to NMC, blue lines in (d) correspond to CM. Parameters are as in Fig. 1.

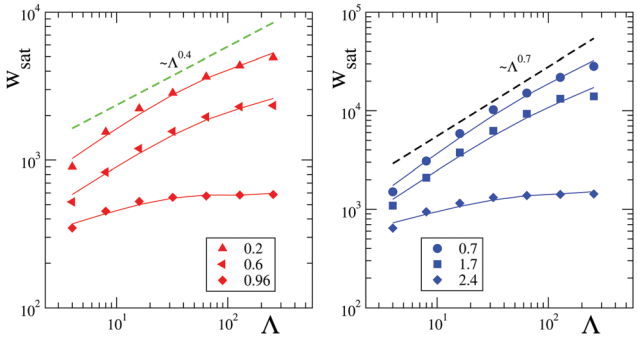

Fig. 7 Roughness order parameters W_{sat} *vs.* Λ for NMC (left panel) and MC (right). Parameters are as in Fig. 1.

we first project the particle distributions in the directions parallel and perpendicular to the measured mean polar order, recalling that in periodic systems LRO is observed for both MC and NMC interactions. We focus here on the orthogonal direction, and analyze the projected one-dimensional system by making a direct analogy with surface growth studies and computing its "fractal" scaling δ as well as its "roughness" W_{sat}. We choose a length Λ, subdivide the projected one-dimensional system into boxes of linear size Λ, and count the number of particles $n(i,\Lambda)$ in each box i. We then compute $\delta(\Lambda) = \sqrt{\langle(n(i,\Lambda) - \langle n\rangle_\Lambda)^2\rangle_i}$ where the average is over the boxes. The dependence of δ on Λ is shown in Fig. 6(c) and (d) for NMC and MC interactions, respectively. Inside the ordered phase, we find that $\delta \propto \Lambda^{0.8}$ for NMC, while $\delta \propto \Lambda^1$ for MC. In the disordered phase the scaling for both types of interactions tends to $\propto \Lambda^{1/2}$. We also perform the measurement of the "roughness" order parameter W_{sat} as a function of Λ for MC and NMC for various noise values η. W_{sat} is obtained, using the projected position of the particles mentioned above, as follows. Each window of size Λ is then subdivided into $\Lambda/\Delta\ell$ tiny boxes, using $\Delta\ell = R_0 = 1$, and we compute the histogram $n_{\Delta\ell}(k)$, where in each tiny box k we count the number of particles. The roughness parameter is then calculated as $W_{sat} = \sqrt{\frac{1}{\Lambda/\Delta\ell}\sum_k (n_{\Delta\ell}(k) - \langle n\rangle)^2}$, where $\langle n\rangle$ denotes the average value of $n_{\Delta\ell}(k)$. The scaling of W_{sat} with Λ, in the ordered phase, is $W_{sat} \propto \Lambda^{0.4}$ for NMC and $W_{sat} \propto \Lambda^{0.7}$ for MC as shown in Fig. 7.

The finding of distinct exponents reveals the existence of fundamental qualitative differences in the spatial arrangement and density fluctuations of particles with MC and NMC interactions, which are also evident upon visual inspection of the snapshots for both types of interactions in Fig. 6(a and b). Finally, the observation that MC leads to larger exponents for δ and W_{sat} with Λ than those for NMC, suggests, together with the existence of a local order-density coupling, that a hypothetical traveling front will experience speed variations across it, that, we speculate, can lead to its destabilization (*i.e.*, prevent band formation).

6 Conclusions

Active systems with velocity alignment, the most studied form of vectorial active matter, have been implemented using both

additive and non-additive interactions[21,22,35–39] under the incorrect assumption that the large-scale properties of the system only depend on the symmetry of interactions, as one expects for an equilibrium system. A first hint that MC and NMC interactions exhibit different pattern forming mechanisms was obtained by the mean-field analysis of both interaction types: the critical noise for the emergence of flocks is independent of the density for NCM interactions, while a clear dependence exists for MC interactions. This implies that the pattern forming coupling between local orientation order and local density leading to density instabilities and band formation operate differently for MC and NMC interactions. Specifically, polar traveling bands, one of the most iconic and controversial features of the Vicsek model, which have been explained invoking a density-order coupling[44] that is present for MC interactions and absent at the mean-field level for NMC, are observed, counterintuitively, for NMC but not for MC interactions. For MC interactions, density instabilities in the direction perpendicular to the (local) polar order (and thus local average velocity) prevent formation of (stable) polar bands. Other significant differences also exist. While systems with MC and NMC interactions exhibit long-range order in periodic boundary conditions, important differences are observed when comparing MC and NMC interactions using reflecting boundary conditions. We find that NMC interactions in confined geometries lead to quasi-long range order, with a critical point that coincides with the one obtained with periodic boundary conditions. For MC interactions, on the other hand, the numerical data suggest the system in confined geometries remains disordered for all noise values. There is a caveat: a significant shift of the critical point is an alternative explanation consistent with the data that cannot be fully excluded; further numerical efforts are required to discern between these two options. Nevertheless, the analysis is conclusive regarding a key point: finite size effects for MC and NMC interactions in confinement are fundamentally different. Finally, density fluctuations also revealed crucial differences between MC and NMC interactions. In particular, the scalings of fluctuations on the projected density show fundamental differences between MC and NMC interactions.

In summary, we have shown that the large-scale properties of active systems with NMC and MC interactions are, despite the common belief, fundamentally different. A direct consequence of this is that correct continuous-time versions of the Vicsek model, which is undoubtedly the cornerstone of active matter, should be formulated using NMC interactions as in ref. 37. Flocking models with MC interactions,[35,36,38] which in ref. 36 were called ''Flying XY spins'', do not exhibit the same behavior of the Vicsek model, and should not be used as a continuum time version of it. Finally, it is worth noting that for incompressible active fluids, argued to be in a different active class than the Vicsek model[45] and the here-studied models, it is likely that the differences between additive and non-additive interactions are less relevant. This observation applies to active systems with dissipative interactions[46] as introduced in ref. 47, whose macroscopic behavior resembles that of an incompressible Vicsek model,[48] as well as active systems interacting by inelastic collisions.[26,49] Further studies are required to clarify this issue.

Conflicts of interest

There are no conflicts to declare.

Acknowledgements

The authors thank D. Bartolo for insightful conversations. O. C. is supported by the Austrian Science Fund (FWF): M 2450-NBL. D. S. acknowledges funding from NSF Grants DMS-1463965 and CBET-1934199. F. P. acknowledges funding from ANR *via* Grant ANR-15-CE30-0002-01, project ''BactPhys''.

References

1 T. Vicsek and A. Zafeiris, *Phys. Rep.*, 2012, **517**, 71–140.
2 M. C. Marchetti, J. F. Joanny, S. Ramaswamy, T. B. Liverpool, M. R. J. Prost and R. A. Simha, *RMP*, 2013, **85**, 1143.
3 T. Sanchez, D. T. Chen, S. J. DeCamp, M. Heymann and Z. Dogic, *Nature*, 2012, **491**, 431–434.
4 Y. Sumino, K. H. Nagai, Y. Shitaka, D. Tanaka, K. Yoshikawa, H. Chaté and K. Oiwa, *Nature*, 2012, **483**, 448–452.
5 V. Schaller, C. Weber, C. Semmrich, E. Frey and A. R. Bausch, *Nature*, 2010, **467**, 73–77.
6 C. Dombrowski, L. Cisneros, S. Chatkaew, R. E. Goldstein and J. O. Kessler, *Phys. Rev. Lett.*, 2004, **93**, 098103.
7 A. Sokolov, I. S. Aranson, J. O. Kessler and R. E. Goldstein, *Phys. Rev. Lett.*, 2007, **98**, 158102.
8 H. Zhang, A. Be'er, E.-L. Florin and H. Swinney, *Proc. Natl. Acad. Sci. U. S. A.*, 2010, **107**, 13526.
9 A. Rabani, G. Ariel and A. Be'er, *PLoS One*, 2013, **8**, e83760.
10 F. Peruani, J. Starruss, V. Jakovljevic, L. Sogaard-Andersen, A. Deutsch and M. Bär, *Phys. Rev. Lett.*, 2012, **108**, 098102.
11 J. Starruss, F. Peruani, V. Jakovljevic, L. Sogaard-Andersen, A. Deutsch and M. Bär, *Interface Focus*, 2012, **2**, 774.
12 K. Kawaguchi, R. Kageyama and M. Sano, *Nature*, 2017, **545**, 327–331.
13 T. B. Saw, A. Doostmohammadi, V. Nier, L. Kocgozlu, S. Thampi, Y. Toyama, P. Marcq, C. T. Lim, J. M. Yeomans and B. Ladoux, *et al.*, *Nature*, 2017, **544**, 212–216.
14 M. Ballerini, *et al.*, *Proc. Natl. Acad. Sci. U. S. A.*, 2008, **105**, 1232–1237.
15 F. Ginelli, F. Peruani, M.-H. Pillot, H. Chaté, G. Theraulaz and R. Bon, *Proc. Natl. Acad. Sci. U. S. A.*, 2015, **112**, 12729–12734.
16 W. Paxton, *et al.*, *J. Am. Chem. Soc.*, 2004, **126**, 13424.
17 N. Mano and A. Heller, *J. Am. Chem. Soc.*, 2005, **127**, 11574.
18 J. Palacci, S. Sacanna, A. P. Steinberg, D. J. Pine and P. M. Chaikin, *Science*, 2013, **339**, 936–940.
19 H.-R. Jiang, N. Yoshinaga and M. Sano, *Phys. Rev. Lett.*, 2010, **105**, 268302.
20 R. Golestanian, T. B. Liverpool and A. Ajdari, *Phys. Rev. Lett.*, 2005, **94**, 220801.

21 A. Bricard, J.-B. Caussin, N. Desreumaux, O. Dauchot and D. Bartolo, *Nature*, 2013, **503**, 95–98.
22 A. Bricard, J.-B. Caussin, D. Das, C. Savoie, V. Chikkadi, K. Shitara, O. Chepizhko, F. Peruani, D. Saintillan and D. Bartolo, *Nat. Commun.*, 2015, **6**, 1–8.
23 A. Kaiser, A. Snezhko and I. S. Aranson, *Sci. Adv.*, 2017, **3**, e1601469.
24 A. Kudrolli, G. Lumay, D. Volfson and L. Tsimring, *Phys. Rev. Lett.*, 2008, **100**, 058001.
25 A. Kudrolli, *Phys. Rev. Lett.*, 2010, **104**, 088001.
26 J. Deseigne, O. Dauchot and H. Chaté, *Phys. Rev. Lett.*, 2010, **105**, 098001.
27 M. Mijalkov, A. McDaniel, J. Wehr and G. Volpe, *Phys. Rev. X*, 2016, **6**, 011008.
28 L. Barberis and F. Peruani, *Phys. Rev. Lett.*, 2016, **117**, 248001.
29 I. S. Aranson, A. Sokolov, J. O. Kessler and R. E. Goldstein, *Phys. Rev. E: Stat., Nonlinear, Soft Matter Phys.*, 2007, **75**, 040901.
30 F. Peruani, A. Deutsch and M. Bär, *Phys. Rev. E: Stat., Nonlinear, Soft Matter Phys.*, 2006, **74**, 030904(R).
31 A. Baskaran and M. Marchetti, *Phys. Rev. Lett.*, 2008, **101**, 268101.
32 S. Weitz, A. Deutsch and F. Peruani, *Phys. Rev. E: Stat., Nonlinear, Soft Matter Phys.*, 2015, **92**, 012322.
33 A. Sokolov, I. S. Aranson, J. O. Kessler and R. E. Goldstein, *Phys. Rev. Lett.*, 2007, **98**, 158102.
34 T. Vicsek, E. A. Czirok, E. B. Jacob, I. Cohen and O. Shochet, *Phys. Rev. Lett.*, 1995, **75**, 1226.
35 F. Peruani, A. Deutsch and M. Bär, *Eur. Phys. J.: Spec. Top.*, 2008, **157**, 111–122.
36 F. D. C. Farrell, M. C. Marchetti, D. Marenduzzo and J. Tailleur, *Phys. Rev. Lett.*, 2012, **108**, 248101.
37 O. Chepizhko, E. G. Altmann and F. Peruani, *Phys. Rev. Lett.*, 2013, **110**, 238101.
38 A. Martín-Gómez, D. Levis, A. Díaz-Guilera and I. Pagonabarraga, *Soft Matter*, 2018, **14**, 2610–2618.
39 P. Degond and S. Motsch, *Math. Models Methods Appl. Sci.*, 2008, **18**, 1193–1215.
40 L. P. Dadhichi, J. Kethapelli, R. Chajwa, S. Ramaswamy and A. Maitra, *Phys. Rev. E*, 2020, **101**, 052601.
41 H. Risken, *The Fokker-Planck equation: methods of solution and applications*, Springer Verlag, Berlin, 1996.
42 J. Barré, R. Chétrite, M. Muratori and F. Peruani, *J. Stat. Phys.*, 2015, **158**, 589–600.
43 H. Chaté, F. Ginelli, G. Grégoire and F. Raynaud, *Phys. Rev. E: Stat., Nonlinear, Soft Matter Phys.*, 2008, **77**, 046113.
44 J.-B. Caussin, A. Solon, A. Peshkov, H. Chaté, T. Dauxois, J. Tailleur, V. Vitelli and D. Bartolo, *Phys. Rev. Lett.*, 2014, **112**, 148102.
45 L. Chen, J. Toner and C. F. Lee, *New J. Phys.*, 2015, **17**, 042002.
46 P. Espanol and M. Revenga, *Phys. Rev. E: Stat., Nonlinear, Soft Matter Phys.*, 2003, **67**, 026705.
47 V. Lobaskin and M. Romenskyy, *Phys. Rev. E: Stat., Nonlinear, Soft Matter Phys.*, 2013, **87**, 052135.
48 M. Romenskyy and V. Lobaskin, *Eur. Phys. J. B*, 2013, **86**, 91.
49 D. Grossman, I. Aranson and E. B. Jacob, *New J. Phys.*, 2008, **10**, 023036.

